Light Output Enhancement of GaN-Based Light-Emitting Diodes by Optimizing SiO_2 Nanorod-Array Depth Patterned Sapphire Substrate

2012 Jpn. J. Appl. Phys. 51 04DG11

(http://iopscience.iop.org/1347-4065/51/4S/04DG11)

Japanese Journal of Applied Physics **51** (2012) 04DG11 **REGULAR PAPER**
DOI: 10.1143/JJAP.51.04DG11

Light Output Enhancement of GaN-Based Light-Emitting Diodes by Optimizing SiO_2 Nanorod-Array Depth Patterned Sapphire Substrate

Ching-Hsueh Chiu, Po-Min Tu, Shih-Pang Chang, Chien-Chung Lin[1]*, Chung-Ying Jang, Zhen-Yu Li, Hung-Chih Yang[2], Hsiao-Wen Zan, Hao-Chung Kuo, Tien-Chang Lu, Shing-Chung Wang, and Chun-Yen Chang[3]

Department of Photonics and Institute of Electro-Optical Engineering, National Chiao Tung University, Hsinchu 30010, Taiwan
[1]*Institute of Photonic System, College of Photonics, National Chiao-Tung University, Guiren Township, Tainan County 71150, Taiwan*
[2]*R&D Division, Epistar Co., Ltd., Science-based Industrial Park, Hsinchu 31040, Taiwan*
[3]*Department of Electronics Engineering, National Chiao Tung University, Hsinchu 30010, Taiwan*

Received September 26, 2011; accepted January 30, 2012; published online April 20, 2012

In this study, we investigated high-efficiency InGaN/GaN light-emitting diodes (LEDs) grown on sapphire substrates with SiO_2 nanorod arrays (NRAs) of different heights. The GaN film showed an improved crystal quality through X-ray diffraction (XRD) full-width at half-maximum (FWHM), photoluminescence (PL), and cathodoluminescence (CL) measurements. The light output power and internal quantum efficiency (IQE) of the fabricated LEDs were increased when compared with those of conventional LEDs. Transmission electron microscopy (TEM) images suggested that the voids between SiO_2 nanorods and the stacking faults introduced during the nanoscale epitaxial lateral overgrowth (NELOG) of GaN can effectively reduce the threading dislocation density (TDD). We believe that the improvements could be attributed to both the enhanced light extraction by utilizing SiO_2 NRAs and the improved crystal quality through the NELOG method. We found that the sample with SiO_2 NRA structures of 200 nm height can increase the LED output power by more than 70% in our study.

1. Introduction

High-brightness GaN-based light-emitting diodes (LEDs) have been extensively applied in large full-color displays, short-haul optical communication, traffic and signal lights, backlight for liquid-crystal displays, and general-purpose light fixtures.[1)] To meet the demand of next-generation applications in projectors, automobile headlights, and high-end light fixtures, further improvements in optical power and external quantum efficiency are required. Typically, heteroepitaxial GaN layers are grown on a planar sapphire substrate by metal-organic chemical vapor deposition (MOCVD).[2,3)] However, currently, GaN-based epilayers still suffer from a high threading dislocation density (approximately 1×10^8–1×10^{10} cm^{-2}) owing to their large lattice mismatch and thermal expansion coefficient misfit.[4)] Previously, numerous investigations revealed that many properties of GaN-based LEDs and/or laser diodes (LDs) are affected by the threading dislocation density (TDD); for example, the efficiency and lifetime of GaN-based LEDs and LDs decrease with increasing TDD of the material. In other words, the carriers in the GaN-based epilayer can leak through these threading dislocations and recombine non-radiatively. Therefore, it is very important to grow high-quality and low-TDD GaN-based epilayers. Previously, there were many attempts to grow an ultraflat-surface, low-TDD, and high-crystal-quality GaN-based epilayer on a sapphire substrate, for example, by epitaxial lateral overgrowth (ELO)[5)] and cantilever epitaxy (CE),[6)] using a microscale SiN_x or SiO_x patterned mask[7–9)] and a patterned sapphire substrate (PSS).[10–14)]

However, it is still difficult to reduce the TDD to a level of $\sim 10^7$ cm^{-2} by these techniques unless a GaN substrate[15)] is used. Recently, nanoscale epitaxial lateral overgrowth (NELOG)[16)] has been found to be a promising method. During the NELOG process, the coalescence overgrowth of nanostructures not only improves crystal quality[17)] but also produces a scattering effect on the emitted photons, leading to a higher light-extraction efficiency (LEE).[18)]

In this study, nanoscale-patterned sapphire substrates with SiO_2 nanorod arrays (NRAs) of different heights are used for the NELOG of the GaN epilayer. As a consequence, the optical and electrical performance characteristics of such devices are improved when compared with those samples grown on planar sapphire substrates. Various oxide heights were considered to fabricate the LEDs, and an optimized SiO_2 NRA height (200 nm) was determined in terms of crystal quality and light output power.

2. Experimental Procedure

The schematic illustration of a GaN LED on sapphire with a SiO_2 NRA process flow chart is shown in Fig. 1. The preparation of sapphire with different SiO_2 NRA depths started with the deposition of 100, 200, and 300 nm SiO_2 on sapphire by plasma-enhanced chemical vapor deposition (PECVD). Then, a 10-nm-thick Ni layer was deposited by an e-gun evaporator. The sample was annealed at 850 °C for 60 s in nitrogen ambient to form self-assembled Ni nano clusters on the SiO_2 layer. The Ni nano clusters acted as etching masks, and reactive ion etching (RIE) and inductive couple plasma (ICP) dry etching were subsequently performed to form SiO_2 NRAs. The height of the SiO_2 NRA on the surface of sapphire was determined by a SiO_2 thickness different from that considered in the PECVD process. The RIE power is 100 W and the etching rate is ~66 nm/min. Thus, the RIE times used were 91, 182, and 273 to dry etch 100, 200, and 300 nm SiO_2 nanorods, respectively. After etching, the SiO_2 NRA was dipped hot HNO_3 to remove the Ni nanoclusters. A conventional GaN LED structure, which consists of ten periods of InGaN/GaN MQWs and a 100-nm-thick p-GaN layer, was deposited by MOCVD. An indium–tin oxide (ITO) layer was used for ohmic contact and current spreading. Lastly, the LED wafers were then processed into LED chips (size: 300×300 μm^2) and packaged in epoxy-free metal cans (TO-46). The output power of the LED was measured by an integrated sphere detector at room temperature.

The optical properties of all samples were investigated in two parts. One is the room temperature photoluminescence (PL) spectrum of u-GaN investigated by 325 nm He–Cd

*E-mail address: chienchunglin@faculty.nctu.edu.tw

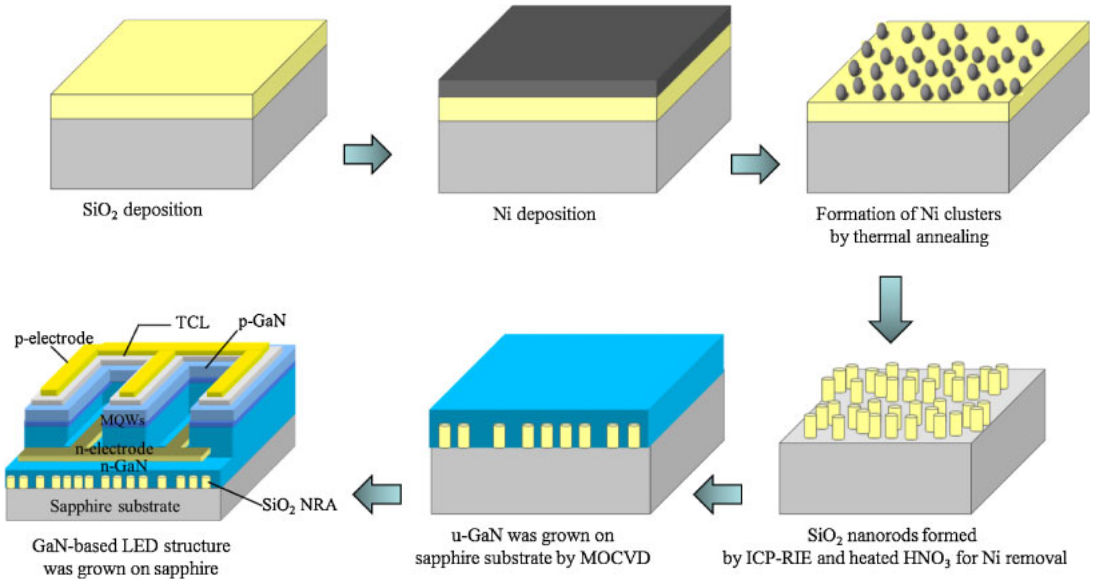

Fig. 1. (Color online) Schematic illustrations of GaN LED grown on sapphire with SiO_2 NRA process flow chart.

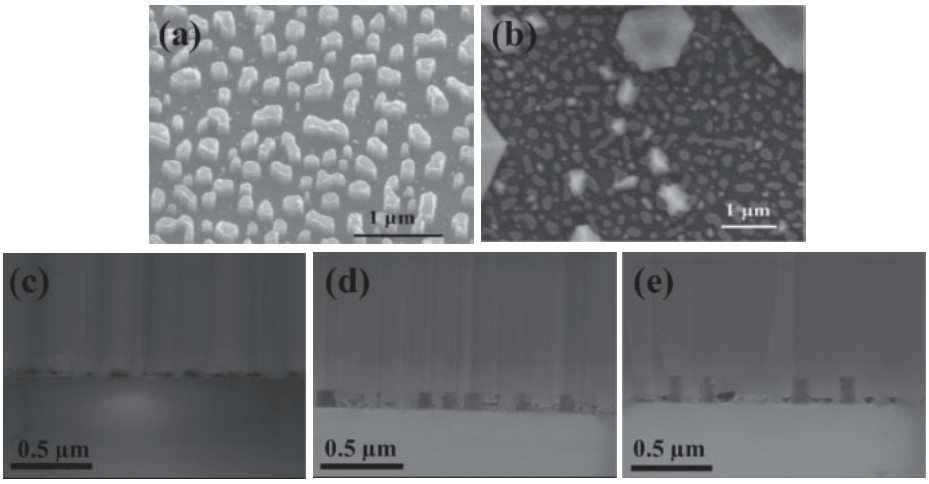

Fig. 2. SEM images of (a) the fabricated SiO_2 NRA (b) GaN nuclei on sapphire with SiO_2 NRAs as growth seeds, and the GaN epilayers on the sapphire with (c) 100, (d) 200, and (e) 300 nm SiO_2 NRAs.

laser excitation. The other is the power-dependent PL measurement. In this case, the PL sample was excited with a frequency-tripled Ti:sapphire laser at a wavelength of 400 nm and a laser output power of 100 mW. The laser pulse width was 200 fs and the repetition rate was 76 MHz. The luminescence spectrum was measured with a 0.5 m monochromator and detected with a photomultiplier tube. The TDD was confirmed by performing cathodoluminescence (CL) measurement. The spatially resolved CL imaging was obtained by scanning electron microscopy (SEM: JEOL 7000F) with a fixed viewing scale. The detailed distribution and threading behaviors of dislocations in the epilayers were then studied by transmission electron microscopy (TEM). Moreover, the details of the interfacial microstructures of the epilayer were obtained by high-resolution TEM. Then, we also carried out the power-dependent PL measurement to estimate the internal quantum efficiency (IQE) of specimens. Finally, after normal clean-room processes, we compared the forward voltage (V) and optical output values (L–I) of LED devices in a conventional probe station and an integrated-sphere setup.

3. Results and Discussion

The SEM image in Fig. 2 indicates that the SiO_2 nanorods were approximately 180–200 nm in diameter. The spacing between the nanorods was about 130–150 nm. Figure 2(a) also shows that the exposed sapphire surface is sufficiently flat for epitaxy. As the deposition process began, localized and hexagonal island like GaN nuclei were first formed on the sapphire surface to initiate GaN overgrowth, as shown in Fig. 2(b). Figures 2(c)–2(e) show the cross-sectional SEM images of the GaN epitaxial layer, where air voids were observed between the SiO_2 nanorods. The existence of the air voids between the nanorods observed from the micrographs suggested that not all the exposed surfaces gained the same growth rate. It is most likely that the regions with

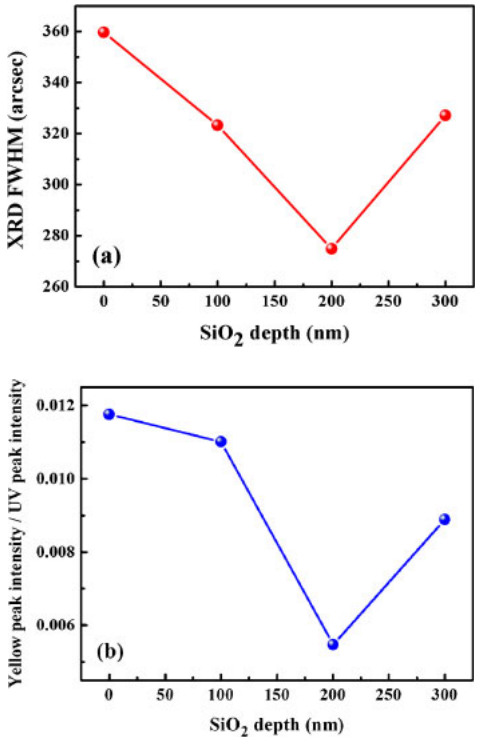

Fig. 3. (Color online) (a) XRD FWHMs of the GaN films grown as a function of the SiO_2 NRA depth; (b) The peak intensity of GaN divided by peak intensity of yellow band as a function of SiO_2 NRA depth.

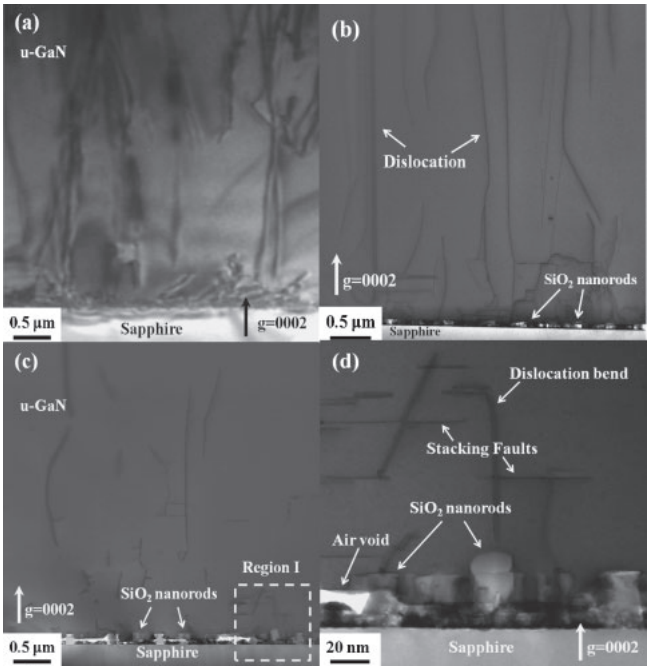

Fig. 4. TEM cross-sectional images of GaN epitaxial layers grown on (a) flat sapphire and sapphire with (b) with 100 and (c) 200 nm SiO_2 NRAs. (d) HRTEM image of region I in (c). The diffraction condition is $g = 0002$.

larger exposed surfaces grow faster, and thus these regions serve as seeding layers and facilitate the lateral coalescence of GaN.

We grew an undoped GaN (u-GaN) epitaxial layer on a flat sapphire surface and a SiO_2 nanorod template. The epitaxial structure comprises a 30-nm-thick GaN nucleation layer and a 2-μm-thick u-GaN epitaxial layer for PL and X-ray diffraction (XRD) measurements. Figure 3(a) shows the XRD full-widths at half-maximum (FWHM) of the u-GaN films on flat sapphire and sapphire with 100, 200, and 300 nm SiO_2 NRAs. The FWHMs of (102) planes, which indicate the densities of edge dislocations,[19] were 360, 323, 275, and 327 arcsec for GaN films on flat sapphire and sapphire with 100, 200, and 300 nm SiO_2 NRAs, respectively. The XRD linewidths of the samples with the SiO_2 NRA template are generally smaller than that of the reference sample, which indicates that the samples with the template have higher crystal quality. The room temperature PL spectrum was also used to analyze the GaN crystal quality. The peak intensity of GaN was divided by the peak intensity of the yellow band (GaN peak/yellow peak), as shown in Fig. 3(b). The intensity of the yellow band is related to defect density. The ratios of the GaN films grown on flat sapphire and sapphire with 100, 200, and 300 nm SiO_2 NRAs were 85, 91, 183, and 113, respectively. The significant decreases in XRD FWHM and increases in GaN peak/yellow peak intensity indicate a reduction in threading dislocation density and thus an overall enhancement material quality. This improvement can be attributed to the strain relaxation of the partially relieved GaN layer in combination with the subsequent regrowth.[20] When the initial GaN epitaxial layer was grown on sapphire, a compressive strain was built up inside the material owing to the mismatched lattice constants and thermal expansion coefficients between GaN and sapphire. These mismatched factors introduced threading dislocations. The NELOG process relaxed the compressive strain. The GaN epitaxial layer acted as a buffer layer to alleviate lattice constant and thermal expansion coefficient mismatches and resulted in an improved crystalline quality. To analyze the detailed epitaxial layer quality, we performed TEM to investigate the cross section of the u-GaN film grown on a flat sapphire surface and a SiO_2 nanorod template.

For the GaN epitaxial layer grown on a flat sapphire surface, the threading dislocation defects propagated vertically from the interface of GaN and sapphire to the top device layers. As a result, the TDD in the conventional GaN layer near the top surface was as high as $10^9\,cm^{-2}$, as shown in Fig. 4(a). When the u-GaN film grew on sapphire with a 100 nm SiO_2 NRA, the NELOG mechanism was not activated owing to the shallow SiO_2 nanorods. As we could see in Fig. 4(b), the dislocations were not bent completely, and they propagated upwards similarly to those on a flat template without any reduction. This situation changed when we increased the rod height to 200 nm. The cross-sectional TEM image of the GaN epitaxial layer grown on sapphire with a 200 nm SiO_2 NRA is shown in Fig. 4(c), and much fewer TDs are observed within the range in view. The dislocation density on the top of the GaN film was calculated to be around $7 \times 10^7\,cm^{-2}$. Figure 4(c) demonstrates the detailed TEM of the epitaxial layers, and the bending and termination of the dislocations can be clearly seen. The reduction in TD density can be attributed to the misfit (mainly perpendicular to the *c*-axis), and dislocation bending occurred just above the voids, as shown in Fig. 4(d). Such behaviors often happened in the NELOG method on a

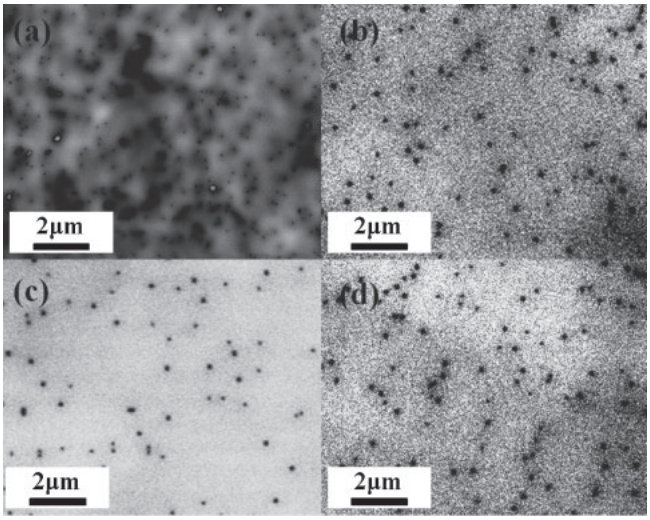

Fig. 5. Top-view CL images of (a) LED I, (b) LED II, (c) LED III, and (d) LED IV.

nanoscale patterned sapphire substrate.[16] On the other hand, when we increased the nanorod height further, we observed that the 300 nm nanorod array is more difficult to coalesce owing to the height of the oxide nanorod, and thus also leads to more coalescent defects. Since these two mechanisms (activation of NELOG and coalescence of GaN) dominate in deep and shallow nanorods, respectively, it is natural to consider that the 200 nm nanorod array exhibits intermediate characteristics and has the highest crystal quality, which is the case in the actual wafer growth.

The LED samples grown on GaN templates without SiO_2 NRAs and with SiO_2 nanorods of 100, 200, and 300 nm heights were represented by LED I, LED II, LED III, and LED IV, respectively. The reduction in dislocation density was also confirmed by CL measurement. Figure 5 shows the plan-view CL emission images of all samples with a 10 kV acceleration voltage at room temperature. LED III shows the least black number of spots among all LED samples. The density of dark regions was estimated to be 3×10^9, 4×10^8, 5.3×10^7, and 2×10^8 cm^{-2} for the LED structures grown on flat sapphire and sapphire with 100, 200, and 300 nm SiO_2 NRAs, respectively. The dark areas in the CL images are regions where minority carriers are consumed by dislocations due to a high nonradiative recombination velocity.[21] From these results, we found the highest crystal quality in the GaN film grown on 200 nm SiO_2.

LED devices with a chip size of 300×300 μm^2 were then fabricated from the completed epitaxial structures with and without SiO_2 NRAs. The forward voltages of LED I, LED II, LED III, and LED IV were 3.61, 3.63, 3.67, and 3.62 V at 20 mA, respectively. The NELOG process had little impact on the LED electrical properties as shown in Table I. On the other hand, the leakage current of LED I, LED II, LED III, and LED IV were 87.5, 36.2, 34.7, and 37.4 nA at a reverse bias voltage of −5 V, respectively. This significant improvement is suggested to originate from the reduction in defect density. Several types of dislocations can contribute to the reverse-bias leakage current,[22] and one of the most dominant types is the screw dislocation.[22,23] The reduction in screw dislocation density can certainly help to

Table I. Forward voltages and leakage currents of all fabricated LEDs.

Sample	Forward voltage (V)	Leakage current (nA)
LED I	3.61	87.5
LED II	3.63	36.2
LED III	3.67	34.7
LED IV	3.62	37.4

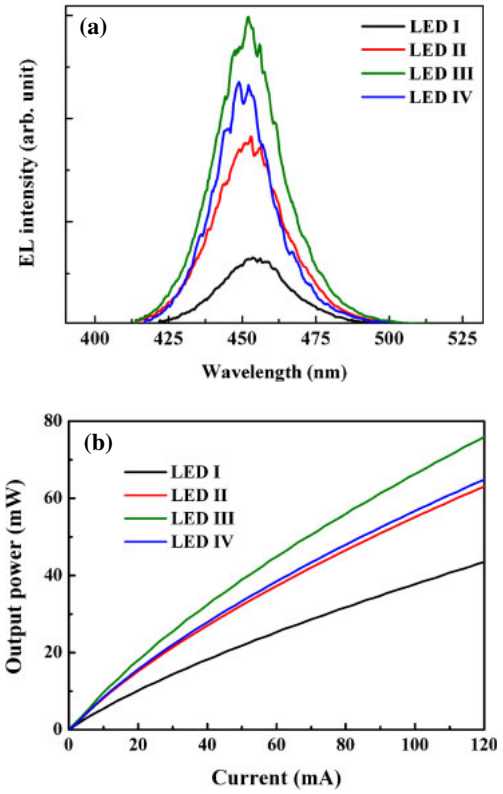

Fig. 6. (Color online) (a) EL spectra. (b) *L–I* curves of GaN-based LEDs grown on sapphire with and without SiO_2 NRAs.

reduce the reverse-bias current. Rosner *et al.* reported that the dark areas in the CL images are regions where minority carriers are consumed by dislocations due to a high nonradiative recombination velocity.[21] Thus, the leakage current of the device was increased by increasing the dislocation density. This indicates an agreement between the TEM and CL results.

The EL peak wavelengths were 454.8, 452.5, 451.4, and 452 nm for LED I, LED II, LED III, and LED IV at a driving current of 20 mA, respectively as shown in Fig. 6(a). The EL wavelength peak blue shift of ~2 nm was observed for the LED structure grown on SiO_2 NRA template. In our previous study, it can be attributed to the compressive strain release by adopting the NELOG scheme.[16] The peak of the EL spectrum shifts to a higher energy owing to quantum-confined Stark effect (QCSE) reduction.[24] The EL wavelength peak blue shift was observed for the LED structure with SiO_2 nanorods, as compared with that grown on planar sapphire. Among samples with different SiO_2 depths, the emission wavelength of LEDs is not affected markedly. Figure 6(b) shows the measured *L–I* curves for LED I,

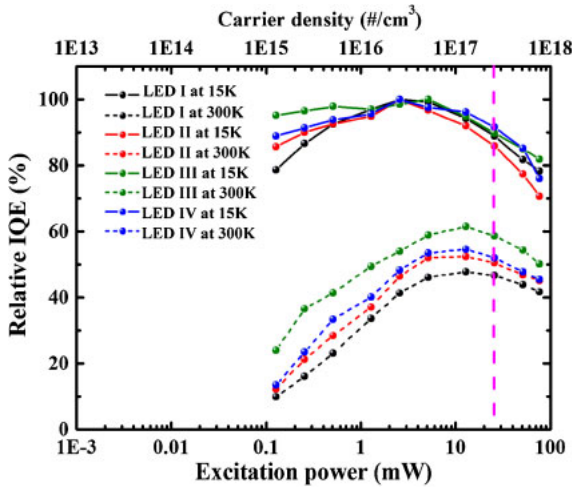

Fig. 7. (Color online) Relative IQE as a function of excitation power for all samples.

LED II, LED III, and LED IV. At an injection current of 20 mA, the light output powers were 10.1, 15.1, 18, and 15.6 mW for LED I, LED II, LED III, and LED IV, respectively. The increases in the light output power of LEDs grown on sapphire with 100, 200, and 300 nm SiO_2 NRAs an injection current of 20 mA were 49.6, 78.2, and 54.4%, respectively, as compared with the LED without SiO_2 NRAs. We believe that the increase in light output power is due to the improved internal quantum efficiency (IQE) and that the light extraction efficiency (LEE). The NRA-assisted NELOG effectively reduced the TDDs of GaN LEDs, which increased the IQE, as we mentioned in the previous section. Moreover, the SiO_2 NRA in the GaN epilayers contributed to light extraction through light scattering at the interface of layer of different refractive indices. Tadatomo *et al.* reported that the output power increased with the patterned sapphire substrate (PSS).[25] Similarly, the extraction efficiency was increased by the SiO_2 NRA in our case.

To appropriately assess the contributions from the IQE enhancement and LEE improvement, we need to perform more measurements. A general approach to evaluating the IQE of LEDs is to compare the integrated PL intensities obtained at low and room temperatures.[26] Figure 7 shows the measured IQE as a function of excitation power at 15 and 300 K for all LED samples. The efficiency is defined as the collected photon number divided by the injected photon number and normalized to the maximum efficiency at 15 K. Usually, the PL excitation intensity is difficult to estimate and it varies between different experiments and wafers. What we would like to do here is to convert the variable pumping intensity into the more common "carrier density". To do that, we could use the equation below to transform our injected power to carrier density:[27]

$$\text{Injected carrier density} = \frac{P}{(h\nu) \times \phi \times d_{\text{active}} \times f} \times \exp(-\alpha_{\text{GaN}} d_{\text{GaN}}) \times [1 - \exp(-\alpha_{\text{InGaN}} d_{\text{active}})] \times (1 - R) \quad (1)$$

The injected carrier density is determined primarily by the power of the pumping laser (P), the energy of the injected photons ($h\nu$), the spot size of the pumping laser (ϕ), the thicknes of GaN and active regions (d_{GaN} and d_{InGaN}), the repetition rate of the pumping laser (f), the absorption efficiency of GaN and InGaN (α_{GaN} and α_{InGaN}), and the reflectance of the pumping laser (R), as expressed by the above equation. Experimentally, we chose $\phi = 50\,\mu\text{m}$, $d_{\text{GaN}} = 75\,\text{nm}$, $d_{\text{active}} = 150\,\text{nm}$, $\alpha_{\text{InGaN}} = 10^5\,\text{cm}^{-1}$, and $R = 0.17$ to calculate the injected carrier density in our samples. The power-ependent PL measurement was performed with a frequency-tripled Ti:sapphire laser at a wavelength of 400 nm and the laser output power ranged from 0.1 to 100 mW. The IQE values of the LEDs grown on planar sapphire and sapphire with 100, 200, and 300 nm SiO_2 NRAs were estimated to be 43.9, 49.9, 54.4, and 48.8%, respectively, at an excitation power of 20 mW (injected carrier density $= 2 \times 10^{17}\,\text{cm}^{-3}$), corresponding to a current of 20 mA. The IQE values of the LEDs grown on sapphire with 100, 200, and 300 nm SiO_2 NRAs were increased by 13.7, 26.9, and 11.2, respectively, as compared that of the LED grown on planar sapphire. We believe that the higher IQE for the LED with SiO_2 NRAs is due to the higher crystalline quality, attributed to the interaction between stacking faults and threading dislocation. Therefore, from the output light power and IQE increases, we can estimate that the LEE increases would be 31.4, 40.4, and 38.8% by the SiO_2 NRA embedded between GaN and sapphire.

4. Conclusions

SiO_2 NRAs of different depths were fabricated by self-assembled Ni clustering, followed by ICP-RIE. The LED grown on sapphire with SiO_2 NRAs demonstrated increases in IQE and LEE when compared with a conventional LED grown on flat sapphire. The TDD reduction in GaN-based epilayers was realized by the SiO_2 NRA-assisted NELOG method. Finally, we can find that the sample with 200 nm SiO_2 NRA structures has the highest crystal quality and light output power enhancement.

Acknowledgments

The authors would like to thank Dr. T. C. Hsu and M. H. Shieh of Epistar Corporation for their technical support. This work was carried out by the National Science Council NSC 98-3114-E-009-002-CC2 in Taiwan, R.O.C.

1) Y. Narukawa, I. Niki, K. Izuno, M. Yamada, Y. Murazki, and T. Mukai: Jpn. J. Appl. Phys. **41** (2002) L371.
2) X. H. Wu, L. M. Brown, D. Kapolnek, S. Keller, B. Keller, S. P. DenBaars, and J. S. Speck: J. Appl. Phys. **80** (1996) 3228.
3) X. H. Wu, D. Kapolnek, E. J. Tarsa, B. Heying, S. Keller, B. P. Keller, U. K. Mishra, S. P. DenBaars, and J. S. Speck: Appl. Phys. Lett. **68** (1996) 1371.
4) C.-H. Chiu, P.-M. Tu, C.-C. Lin, D.-W. Lin, Z.-Y. Li, K.-L. Chuang, J.-R. Chang, T.-C. Lu, H.-W. Zan, C.-Y. Chen, H.-C. Kuo, S.-C. Wang, C.-Y. Chang, C.-H. Chiu, P.-M. Tu, D.-W. Lin, Z.-Y. Li, T.-C. Lu, H.-W. Zan, H.-C. Kuo, and S.-C. Wang: IEEE J. Sel. Top. Quantum Electron. **17** (2011) 971.
5) D. Kapolnek, S. Keller, R. Vetury, R. D. Underwood, P. Kozodoy, S. P. DenBaars, and U. K. Mishra: Appl. Phys. Lett. **71** (1997) 1204.
6) D. M. Follstaedt, P. P. Provencio, N. A. Missert, C. C. Mitchell, D. D. Koleske, A. A. Allerma, and C. I. H. Ashby: Appl. Phys. Lett. **81** (2002) 2758.

7) A. Sakai, H. Sunakawa, and A. Usui: Appl. Phys. Lett. **71** (1997) 2259.
8) T. S. Zheleva, O. H. Nam, M. D. Bremser, and R. F. Davis: Appl. Phys. Lett. **71** (1997) 2472.
9) D. S. Wuu, W. K. Wang, K. S. Wen, S. C. Huang, S. H. Lin, S. Y. Huang, C. F. Lin, and R. H. Horng: Appl. Phys. Lett. **89** (2006) 161105.
10) Y. J. Lee, J. M. Hwang, T. C. Hsu, M. H. Hsieh, M. J. Jou, B. J. Lee, T. C. Lu, H. C. Kuo, and S. C. Wang: IEEE Photonics Technol. Lett. **18** (2006) 1152.
11) Z. H. Feng, Y. D. Qi, Z. D. Lu, and K. M. Lau: J. Cryst. Growth **272** (2004) 327.
12) T. V. Cuong, H. S. Cheong, H. G. Kim, H. Y. Kim, C.-H. Hong, E. K. Suh, H. K. Cho, and B. H. Kong: Appl. Phys. Lett. **90** (2007) 131107.
13) H. Gao, F. Yan, Y. Zhang, J. Li, Y. Zeng, and G. Wang: J. Appl. Phys. **103** (2008) 014314.
14) D. S. Wuu, W. K. Wang, K. S. Wen, S. C. Huang, S. H. Lin, R. H. Horng, Y. S. Yu, and M. H. Pan: J. Electrochem. Soc. **153** (2006) G765.
15) S. Nagahama, N. Iwasa, M. Senoh, T. Matsusgita, Y. Sugimoto, H. Kiyoku, T. Kozaki, M. Sano, H. Matsumura, H. Umemoto, K. Chocho, and T. Mukai: Jpn. J. Appl. Phys. **39** (2000) L647.
16) C. H. Chiu, Z. Yu. Li, C. L. Chao, M. H. Lo, H. C. Kuo, P. C. Yu, T. C. Lu, S. C. Wang, K. M. Lau, and S. J. Cheng: J. Cryst. Growth **310** (2008) 5170.
17) T.-Y. Tang, C.-H. Lin, Y.-S. Chen, W.-Y. Shiao, W.-M. Chang, C.-H. Liao, K.-C. Shen, and C.-C. Yang: IEEE Trans. Electron Devices **57** (2010) 71.
18) C. H. Kuo, L. C. Chang, C. W. Kuo, and G. C. Chi: IEEE Photonics Technol. Lett. **22** (2010) 257.
19) H. Heinke, V. Kirchner, S. Einfeldt, and D. Hommel: Appl. Phys. Lett. **77** (2000) 2145.
20) C. H. Chiu, D. W. Lin, Z. Y. Li, C. H. Chiu, C. L. Chao, C. C. Tu, H. C. Kuo, T. C. Lu, and S. C. Wang: Jpn. J. Appl. Phys. **49** (2010) 105501.
21) S. J. Rosner, E. C. Carr, M. J. Ludowise, G. Girolami, and H. I. Erikson: Appl. Phys. Lett. **70** (1997) 420.
22) E. J. Miller, E. T. Yu, P. Waltereit, and J. S. Speck: Appl. Phys. Lett. **84** (2004) 535.
23) E. G. Brazel, M. A. Chin, and V. Narayanamurti: Appl. Phys. Lett. **74** (1999) 2367.
24) S. F. Chichibu, A. C. Abare, M. P. Minsky, T. Deguchi, D. Cohen, P. Kozodoy, S. B. Fleischer, S. Keller, J. E. Bowers, E. Hu, U. K. Mishra, L. A. Coldren, S. P. DenBaars, K. Wada, T. Sota, and S. Nakamura: Mater. Sci. Eng. B **59** (1999) 298.
25) K. Tadatomo, H. Okagawa, Y. Ohuchi, T. Tsunekawa, Y. Imada, M. Kato, and T. Taguchi: Jpn. J. Appl. Phys. **40** (2001) L583.
26) S. Watanabe, N. Yamada, M. Nagashima, Y. Ueki, C. Sasaki, Y. Tamada, T. Taguchi, and H. Kudo: Appl. Phys. Lett. **83** (2003) 4906.
27) Y. J. Lee, C. H. Chiu, C. C. Ke, P. C. Lin, T. C. Lu, H. C. Kuo, and S.-C. Wang: IEEE J. Sel. Top. Quantum Electron. **15** (2009) 1137.